Remote Sens. **2011**, *3*, 2440-2460; doi:10.3390/rs3112440

OPEN ACCESS

Remote Sensing

ISSN 2072-4292

www.mdpi.com/journal/remotesensing

Article

An Object-Based Classification of Mangroves Using a Hybrid Decision Tree—Support Vector Machine Approach

Benjamin W. Heumann †

Department of Geography and Center for Galapagos Studies, University of North Carolina at Chapel Hill, Campus Box 3220, Chapel Hill, NC 27599, USA

† Current Address: Department of Geography and Global Environmental and Climate Change Centre, McGill University, Burnside Hall Room 705, 805 Sherbrooke St. West, Montreal, QC H3A 2K6, Canada; E-Mail: benjamin.heumann@mail.mcgill.ca

Received: 20 September 2011; in revised form: 8 November 2011 / Accepted: 10 November 2011 / Published: 17 November 2011

Abstract: Mangroves provide valuable ecosystem goods and services such as carbon sequestration, habitat for terrestrial and marine fauna, and coastal hazard mitigation. The use of satellite remote sensing to map mangroves has become widespread as it can provide accurate, efficient, and repeatable assessments. Traditional remote sensing approaches have failed to accurately map fringe mangroves and true mangrove species due to relatively coarse spatial resolution and/or spectral confusion with landward vegetation. This study demonstrates the use of the new Worldview-2 sensor, Object-based image analysis (OBIA), and support vector machine (SVM) classification to overcome both of these limitations. An exploratory spectral separability showed that individual mangrove species could not be spectrally separated, but a distinction between true and associate mangrove species could be made. An OBIA classification was used that combined a decision-tree classification with the machine-learning SVM classification. Results showed an overall accuracy greater than 94% (kappa = 0.863) for classifying true mangroves species and other dense coastal vegetation at the object level. There remain serious challenges to accurately mapping fringe mangroves using remote sensing data due to spectral similarity of mangrove and associate species, lack of clear zonation between species, and mixed pixel effects, especially when vegetation is sparse or degraded.

Keywords: mangroves; OBIA; support vector machine; Galapagos Islands; decision-tree; classification

1. Introduction

1.1. Context

Mangroves are an assemblage of tropical and sub-tropical halophytes (*i.e.*, salt tolerant) woody plants. Mangrove forests are among the most productive forest ecosystems in the world and unique in linking terrestrial and marine systems through the inter-tidal zone [1]. Despite the low tree species diversity and simple canopy structure, mangroves provide many valuable ecosystems goods and services such as carbon sequestration, habitat for terrestrial fauna as well as economically important fisheries, and coastal hazard mitigation [2]. Mangrove forests can range from vast swamps across large estuarine systems such as the Ganges River Delta to strips of vegetation along the fringe of arid coastlines.

Globally, satellite remote sensing has played an important role in mapping and monitoring mangroves [3,4]. Mapping and monitoring mangrove forests is critically important for numerous scientific areas such as carbon stock estimates of tropical coastal nations, effectively managing commercial fisheries and their mangrove nurseries, and understanding the dynamics of vegetation-coastal geomorphology and coastal hazard mitigation. Furthermore, mangroves can provide unique habitat for rare species such as the mangrove finch in the Galapagos Islands of Ecuador.

Previous studies have reported remote sensing classification accuracies between mangroves and other landcover ranging from 75% to 90%, though many studies have omitted accuracy assessments (see [4] for an in-depth review of satellite remote sensing or [5] for a more general review). There remain a number of challenges to accurately detect mangroves including spectral similarity between mangroves and nearby landward tropical vegetation including in arid or marginal environments [6-9] and the effect of mixed pixels for fringe mangroves [10]. Detection of individual mangrove species presents an even greater challenge. Traditional remote sensing approaches generally have failed to detect individual species [11]. While Vaiphasa *et al.* [12] and Wang and Sousa [13] were able to discriminate between mangrove species in hyperspectral laboratory studies, real-world results have been mixed. Almost all recent studies utilize very high resolution imagery, though a wide variety of different techniques have been tested including fuzzy classifications [14], neural networks [15,16], support machine vectors [17], post-classification data fusion [18] and OBIA [15,19-21]. Studies using only multispectral data have generally reported moderate to poor results. For example, Neukermans *et al.* [14] report an overall accuracy of 72 percent based on the mapping of four mangrove species and the surrounding land cover using Quickbird multispectral imagery and a fuzzy classification scheme. Similarly, Wang *et al.* [19] report an overall classification accuracy of nearly 75 percent or less for each of three mangrove species using Quickbird or IKONOS imagery with a maximum likelihood classification (MLC) technique.

The incorporation of spatial information either in the form of OBIA or pixel-based image texture (e.g., grey-level co-occurrence matrix or lacunarity) improves the classification accuracy [15-17,19,20]. Spatial information seeks to extract repeated patterns in canopy structure that can be indirectly related to species. This approach has merit as mangrove genera often differ greatly in form and structure [22]. Spatial metrics are very sensitive to edge effects and work best over continuous canopies. In the case of fringe or basin mangroves, mangrove species zonation is often not as distinct as in other

environments, and high edge length to area ratio makes edge effects a serious challenge. Thus, to effectively map and monitor fringe mangrove forests, especially at local and regional scales, the challenges of spectral confusion and likely limited effectiveness of spatial metrics are constraining factors. Previous studies have reported a range of classification accuracies. Wang *et al*. [15] report that a hybrid OBIA-MLC classification outperforms either individual approach, but accuracy for individual species still ranged from 74% to 98%. Both Huang *et al.* [17] and Myint *et al.* [20] report accuracies greater than 90% using spatial data as part of the classification, or as an input into the image object segmentation process.

1.2. Study Objective

The objective of this study was to map fringe and basin mangrove forests at the species level. First, an analysis of spectral separability of vegetation using Jeffries-Matusita separability measure was conducted to distinguish between vegetation types or groups and to evaluate the differences between Quickbird and Woldview-2 for multispectral analysis. Based on these results, a hybrid OBIA-SVM approach was designed to enhance vegetation separability. An object-based decision tree classification was used to classify classes other than dense coastal vegetation that are not central to this study. A support vector machine classification was used to classify dense coastal vegetation between true mangroves and mangrove associates. The accuracy of the results was analyzed at the object level and field plot or point level for individual vegetation types.

1.3. Background—Object Based Image Analysis

Pixel-based analysis is generally conceptually simple and methods are generic across sensors. However, pixels are often not the unit of interests, but rather the default unit of measurement. For example, individual crowns and canopy gaps consist of multiple pixels and produce spatial-autocorrelation within objects that can be detected using high resolution imagery [23]. OBIA seeks to create "meaningful" objects by segmenting an image into groups of pixels with similar characteristics based on spectral and spatial properties [24]. In OBIA, segmented objects become the unit of analysis, from which spectral statistics, such as spectral band means and standard deviation, or spatial information, such as image texture, can be used for further analysis including image classification. In the software eCognition, user-defined scale, shape, and compactness parameters make OBIA particularly useful for creating objects with heterogeneous pixels such as desert with sparse vegetation. OBIA has been widely applied for forest remote sensing studies [25-28] and has been successfully applied to mangrove studies [15,20,29]. However, OBIA has not been explicitly applied to fringe mangroves.

1.4. Background—Support Vector Machine

SVM is a machine-learning technique that is well adapted to solving non-linear, high dimensional space classifications [30]. For remote sensing, SVM is a useful tool for multispectral and hyperspectral classifications in which spectral separability is less than perfect. The mathematical formulation of SVM is described by Vapnik [31] and a detailed assessment of SVM for remote sensing is described

by Huang *et al.* [32]. Though still a novel method for remote sensing, SVM has been applied in many other fields such as biology, biochemistry, and economics. SVM differs from traditional classification approaches by identifying the boundary between classes in n-dimensional spectral-space rather that assigning points to a class based on mean values. SVM creates a hyperplane through n-dimensional spectral-space that separates classes based on a user defined kernel function and parameters that are optimized using machine-learning to maximize the margin from the closest point to the hyperplane. Figure 1 illustrates the difference between a maximum likelihood classification and a SMV. By identifying the hyperplane that separates two classes (represented by the red and blue dots) rather than using the distance between class spectral means (the black dots), SVM can produce a more accurate classification. A penalty parameter allows the SVM to vary the degree of training data misclassified due to possible data error when optimizing the hyperplane. While there are many possible kernels, four common kernels found in remote sensing packages are linear, polynomial, radial basis function, and sigmoid. Finding the best kernel and parameters can be difficult, though Hsu *et al.* [33] suggest starting with a radial basis function and testing a range of parameters to identify an effective model. In a recent study by Yang [34], it is shown that for most land cover classes, the radial basis function is the best kernel with a penalty parameter of 100.

Figure 1. A stylized example of a cluster-type **(left)** and support vector machine likelihood classification **(right)** between two hypothetical classes shown in blue and red.

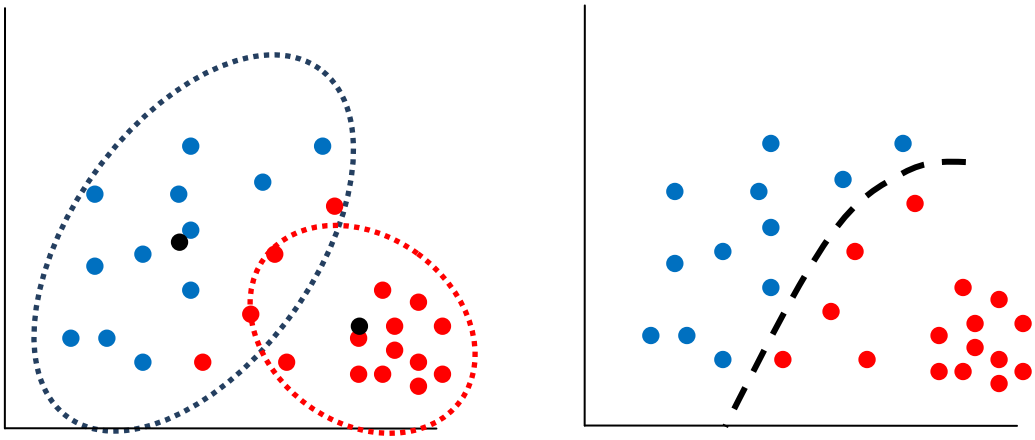

Several studies have demonstrated the great potential for SVM. Pal and Mather [30] found that SVM outperforms maximum likelihood and artificial neural network classifiers using Landsat TM and is well suited for small training sets and high-dimensional data. Foody and Mathur [35] found SVM outperforms discriminate analysis and decision-tree algorithms for airborne sensor data. Li *et al.* [36] applied SVM to an OBIA with better results than standard fuzzy logic classification. Only a single study has applied SVM for analysis of mangroves. Huang *et al.* [17] applied SVM as part of a fusion methodology of spectral and image texture data to map mangroves although the effectiveness of SVM for multispectral classification of mangroves remains untested.

2. Methodology

2.1. Study Area

The research was conducted on Isabela Island in the Galapagos Archipelago, Ecuador. The Galapagos Islands, located 1,000-km off the coast of Ecuador, are an archipelago consisting of 13 large islands, 4 of which have human populations, and 188 small islands and rocks (Figure 2). The Galapagos Islands were declared a national park in 1959 (the park consists of 97% of land area), a UNESCO World Heritage Site in 1978, and a UNESCO Biosphere Reserve in 1987. The Galapagos Islands lie on the western edge of the Atlantic-East Pacific mangrove complex. Mangrove forests consist of three true species common in this region: Rhizophora mangle (red), Avicennia germinans (black), and Laguncularia racemosa (white), and as well as the associate species such as Conocarpus erectus (button or buttonwood mangrove) and Hippomane mancinella (manzanillo), or other halophytes growing on nearby sand flats or dunes [37].

Figure 2. Quickbird false color composites for the Puerto Villamil and Cartago study areas on Isabela Island in the Galapagos Islands.

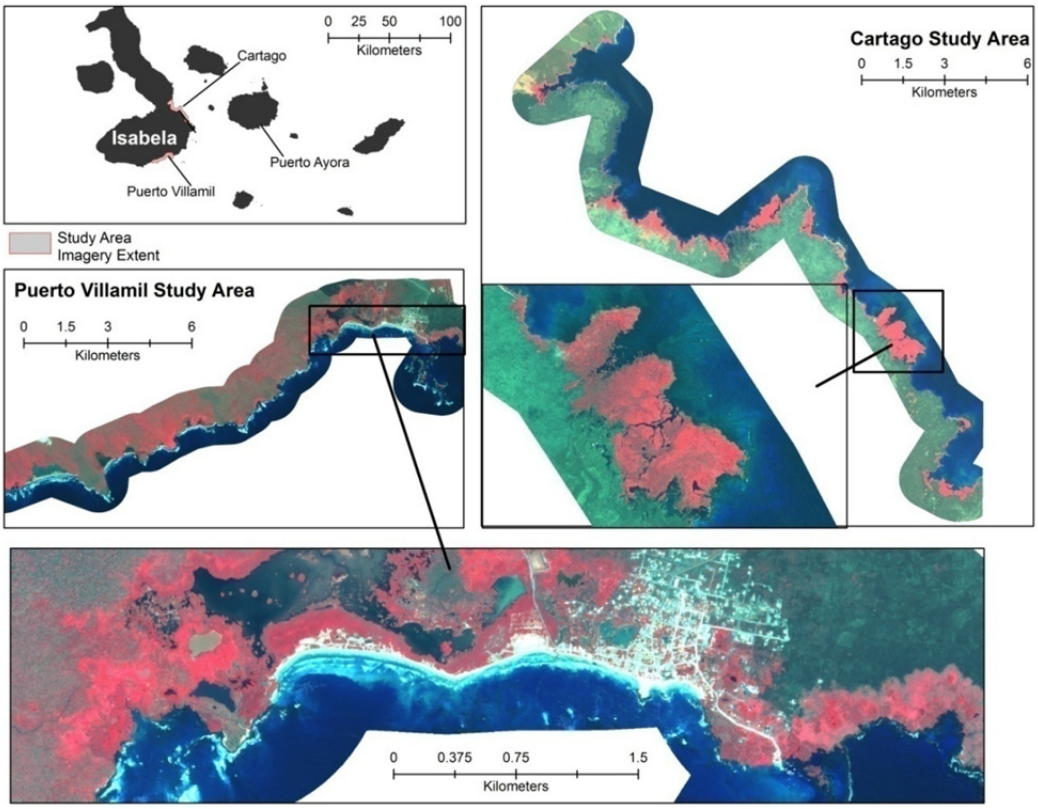

In the Galapagos Islands, mangrove forest form dense, but small patches in protected coves and lagoons along an otherwise barren or arid coast. Mangrove forests in the study site can be described primarily as fringe mangroves forming along the coastline or basin mangroves along hyper-saline lagoons. Mangroves grow on a range of substrates from aa lava to sand or silty-clay. For a more detailed description of the arid coastal environment in the Galapagos Islands, see Van der Werff and Andersen [37].

Figure 3. Examples of vegetation near Puerto Villamil (from upper left, clockwise): **(A)** tall black mangroves near a fresh water spring, **(B)** red mangroves growing on lava shoreline, **(C)** mixed arid vegetation and mangroves along a hyper-saline pond, **(D)** tall red mangroves mixed with white and black mangroves on a saline pond.

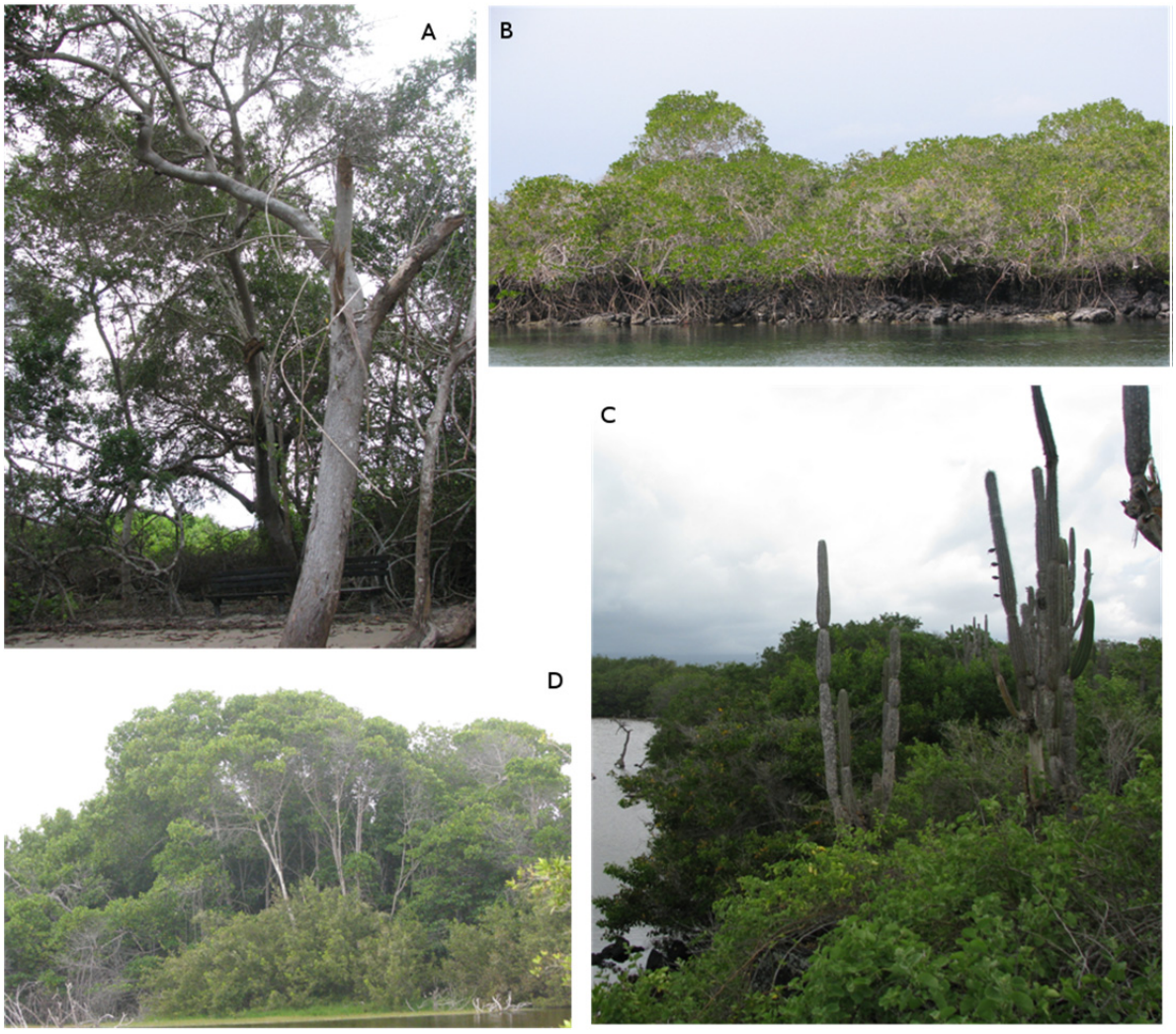

This study focuses on two study areas on Isabela Island: Puerto Villamil and Cartago (Figure 2). The Puerto Villamil study site is located on the southern end of Isabela Island extending west from the town of Puerto Villamil. The study area contains some features unique to the Galapagos Islands including the largest lagoon complex in the Galapagos Islands, the longest sand beach, and complex geologic topography along the coastline. Figure 3 shows several examples of the mangroves in different settings from the study area. Salinity varies greatly across the study site as both fresh water springs and hyper-saline ponds occur in relatively close proximity. Field observations show that while mangrove species form patterns of zonation based on salinity and/or wave action, the mangrove and associate species co-occur in close proximity due to micro-topographical geological features (*i.e.*, lava coastline). To the west of Puerto Villamil, the elevation increases quickly away from the shoreline towards the Sierra Negra or Cerro Azul volcanoes and the vegetation changes from barren/arid to semi-arid/semi-humid along this elevation transition. It is important to note that unlike large riverine mangrove forests like those along the coast of mainland Ecuador, the pattern of zonation between

mangrove and mangrove associate species is truncated and highly variable due to the small inter-tidal zone and the geologic rather the fluvial coastal geomorphology. The Cartago study area is located on the eastern edge of Isabela Island. This area has the largest mangrove forest patches in the Galapagos. Unlike the Puerto Villamil study area, Cartago lacks lagoons or vegetation away from the coast as the study area lies on a relatively flat lava field to the east of Sierra Negra.

2.2. Field Data

Field data were collected during the summer of 2009 near the town of Puerto Villamil. Due to conservation policies within the Galapagos National Park, non-destructive sampling was required. Mangroves form stands with dense aerial roots and branches, making many areas inaccessible. An opportunistic sampling scheme was conducted due to logistical constraints and efforts were made to sample a wide range of conditions for each species (Table 1). A wide range of conditions were sampled from lava to sand substrates, fresh water springs to hypersaline ponds, and short shrubs to trees over 20 m tall. Canopy height, substrate conditions, and mangrove species were recorded at nine points for 48, 10-m diameter plot. Plot location was recorded using a Trimble GeoXT GPS unit and differentially corrected to a 95% horizontal positional accuracy of less than 1.5 m. To extend the extent of the sampled area, an additional 481 species and height point measurements were collected Point locations were measured using a compass and laser range finder from a known GPS position. Due to the limited accuracy of the analog compass (±1°), a maximum of 100 m from the observer was set for all points collected. All field data points are considered representative for a 3-m diameter circle.

Table 1. Vegetation field data by species at plots and individual points.

	Species	Plots*	Points	Total	Percent
MA (Mangrove Associates)	AC (Acacia)	8	27	35	3.472
	MZ (Manzanillo)	43	7	50	4.960
	OV (Other Vegetation)	16	17	33	3.274
	BW (Buttonwood)	56	55	111	11.012
TM (True Mangroves)	RM (Red Mangrove)	120	174	294	29.167
	WM (White Mangrove)	146	243	389	38.591
	BM (Black Mangrove)	66	30	96	9.524
	Total	**455**	**553**	**1,008**	

2.3. Remote Sensing Data

Details of the Quickbird and Worldview-2 imagery are shown in Table 2. The Quickbird imagery was cloud-free over coastal areas, while the Worldview-2 imagery had a few clouds over the study area. Thus, the Quickbird imagery was used for the first level of analysis. All imagery was geometrically corrected using the ENVI Rational polynomial coefficients (RPC) with ground control points (GCP) orthorectification correction algorithm. Since all mangroves grow within the inter-tidal zone, the elevation was assumed to be at mean sea-level across the image. The root mean square error (RMSE) was found to be less than 1.5 m using 16 independent GCPs. All imagery was radiometrically corrected using a Dark Object Subtraction. Since consistent dark objects could not be identified between images, a 1% threshold value for each band was used. Solar angle was not found to be

substantially different between images. All imagery was resampled to a resolution of 2 m using a cubic convolution interpolation. Several band ratios were computed to assist with classification. Band ratios were selected based on exploratory analysis using visual interpretation and the feature optimization tool in eCognition. The selected band ratios were NIR/Red (*i.e.*, Simple Ratio) and NIR/Blue for the Quickbird imagery, and NIR2/Red, Red Edge/Green, and Yellow/Coastal Blue for the Worldview-2 imagery.

Table 2. Imagery details for the Quickbird and Worldview-2 sensors.

Sensor	Quickbird	Worldview-2
Acquisition Date	27 August 2008	01 October 2010
Spatial Resolution (m)		
Pan	0.6	0.5
MSS	2.4	2.0
Spectral Channels (nm)		
Coastal Blue	N/A	400–450
Blue	450–520	450–510
Green	520–600	510–580
Yellow	N/A	585–625
Red	630–690	630–690
Red Edge	N/A	705–745
NIR-1	760–900	770–895
NIR-2	N/A	860–1,040

2.4. Spectral Separability

Spectral separability analysis compares the spectral signature of classes and determines the degree to which those classes can be distinguished. Spectral separability analysis is a commonly used exploratory analysis approach for selecting classes and training data for classification. Spectral separability was calculated using Jeffries-Matusita (J-M) Distance that measures the divergence between spectral means [38,39]. The J-M distances in ENVI is squared so that the distance values range from 0 to 2, where values greater than 1.9 are highly separable, and value less than 1.0 require class clumping or new training data for traditional mean-based classification methods.

2.5. Object-Based Image Analysis

Image segmentation and decision-tree classification were conducted using eCognition Developer 8. eCognition groups pixels based on spectral and spatial properties [24]. A two-level segmentation was used to first classify general land cover classes, and then refine the coastal vegetation classes. The first-level segmentation used shape = 0.5, compactness = 0.5, and scale = 25. The object size varied based on the heterogeneity of the area and the land cover class. For example, lava objects had a mean area of 656 m^2, with a standard deviation of 625 m^2 compared ocean objects had a mean area of 1,385 m^2 with a standard deviation of 1,926 m^2. A second image level was segmented based on the Worldview-2 imagery using shape = 0.5, compactness = 0.9, and scale = 10 for only the dense coastal vegetation classification from level 1. The mean level 1 object size was 144 m^2 with a standard deviation of 102 m^2.

2.5.1. Decision-Tree Classification

The decision tree classification is shown in Figure 4. Class rules were identified using interactive visual interpretation of threshold values based on training data, existing map, and expert knowledge of the study area. Upland and coastal vegetation were separated using a distance rule of 250 m from open water based on field observations. While there was little confusion between these general land cover classes, there was considerable confusion between lava and shallow water over lava (e.g., ponds, coastline). In these cases, objects were manually edited using expert image interpretation.

Figure 4. Object-based image analysis (OBIA) Decision Tree (rectangle = image; diamond = rule; oval = class).

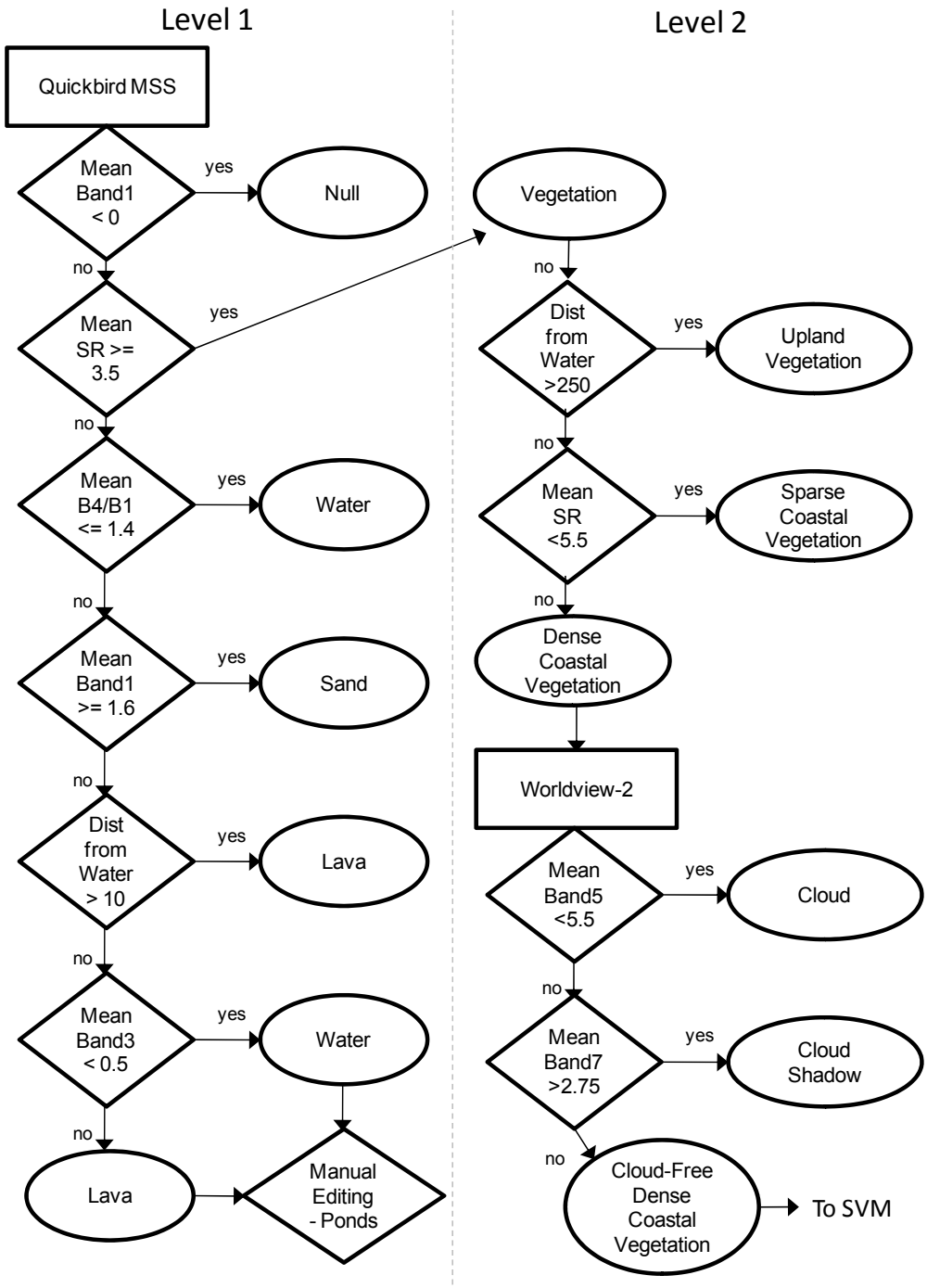

Although overall cloud cover was less than 15% in the Worldview-2 image, clouds and cloud-shadow were classified and removed from the vegetation analysis. The remaining dense coastal vegetation objects were exported to ArcGIS 9.3.1 with the mean values of each band and band ratio for each object. In ArcGIS, the shapefiles were converted to raster stacks for analysis in ENVI 4.8. It should be noted that during exploratory analysis, object-level standard deviation and texture (*i.e.*, grey-level co-occurrence matrix) were also calculated, but they were not found to substantially improve classification results, while raising concerns of model over-fitting with higher data dimensionality. Additionally, the eCognition fuzzy nearest neighbor classification, using the feature optimization tool to select input data for the classification, did not produce acceptable results for the true mangrove classification. When using only mean spectral information, there was insufficient separability between classes. The addition of standard deviation or skewness of spectral data or image texture, separability increased, but classification results showed strong overfitting of the classification to training data.

2.5.2. Support Vector Machine Classification

The SVM classification was conducted using ENVI. Calibration and validation objects were selected based on field data; homogenous objects were verified through visual assessment. The distribution of the objects is shown in Table 3. The objects were systematically divided between calibration and validation datasets based on the object ID created systematically across the image during segmentation. This ensured an equivalent geographic distribution of calibration and validation data. An SVM radial basis function (RBF) kernel was applied using the default parameters (gamma = 0.091 and a penalty parameter of 100). The penalty parameter is particularly important for non-separable classes. Equation (1) shows the RBF kernel:

$$K(xi,xj) = \exp(-g||xi - xj||2),\ g > 0 \quad (1)$$

where g is the user-defined gamma.

ENVI conducts pair-wise iterations of SVM and assigns fuzzy class membership. Classes are assigned using the highest membership. Exploratory analysis did not show improved results with other gamma or penalty values.

Table 3. Distribution of objects used to calibrate and validate the support vector machine (SVM) classification.

	True Mangroves	Mangrove Associates	Total
Calibration	143	54	197
Validation	73	24	101
Total	216	78	298

2.6. Accuracy Assessment

The accuracy of the SVM classification was assessed in several ways. First, accuracy is assessed at the object-level using an error confusion matrix. The overall, producer's, and user's accuracy was calculated, in addition to the kappa statistic. The area under the curve (AUC) of the receiver operating characteristic (ROC) was also computed based on fuzzy membership [40]. This statistic illustrates the

accuracy of the classification relative to a perfect classification (AUC = 1) and a random classification (AUC = 0.5) based on the rate of false positives. Second, an error confusion matrix was created for the individual vegetation types at the field point level and all classes from both the decision tree and SVM classification. To further illustrate the relationship between the field data and SVM, a boxplot distribution of fuzzy membership to true mangroves was computed for each field vegetation class.

3. Results and Discussion

3.1. Spectral Separability Analysis

Class spectral separability at the pixel level for all vegetation field data points is shown in Table 4 for the Quickbird (A) and Woldview-2 (B) imagery. The spectral separability between vegetation classes for the Quickbird imagery was moderate to poor. Not a single value was found to be greater than the suggested threshold of 1.9, though many values were greater than 1.8. More importantly, there was not a consistently high separability for any individual species. This indicates that the ability to discriminate vegetation types with high accuracy using Quickbird imagery is very unlikely. Although the Worldview-2 imagery had better spectral separability than the Quickbird imagery (Table 3(C)), likely due to the greater number of spectral bands, only manzanillo (MZ) was consistently separable from mangroves. Separability between mangrove species was particularly low, especially between red and white mangroves. This result is consistent with field measurements taken from a handheld spectroradiometer during the field campaign [41]. The spectral overlap and confusion between species was consistent with the accuracy assessment of previous studies using various classification techniques. Neukermans *et al.* [14] reported an overall accuracy of 72% using a fuzzy classification and Wang *et al.* [19] reported an overall accuracy of 75% using a maximum likelihood technique, although the user's accuracy for some species was as low as 55%. During the exploratory analysis of this study, a MLC classification failed to detect two separate true mangrove and mangrove associate classes.

Table 4(D) shows spectral separability of true mangroves (TM) and mangrove associates (MA) for all vegetation field points and dense vegetation objects from OBIA segmentation and decision tree classification. In most cases, spectral separability increased with the inclusion of band ratios and spatial information through image segmentation into objects. However, the maximum value of 1.665 demonstrates that there is considerable spectral overlap between the two classes and that non-traditional classification methods are likely required (*i.e.*, SVM). The use of an object-based approach worked best for dense vegetation objects. Results for sparse vegetation objects (not shown) did not improve the separability results and were sometimes worse than the pixel-based analysis due to the inclusion of background substrate reflectance. Moreover, the moderate to poor spectral separability indicates the in ability to discern between species using this imagery which includes noise from non-leaf surfaces such as braches and background substrate. Given, pure leaf reflectance from finer scale imagery or spectral unmixing, spectral separability may be higher.

Table 4. Spectral Separability (Jeffries-Matustia Distance) for individual species using Quickbird **(A)** or Worldview-2 **(B)** imagery, the difference between the Quickbird and Worldview-2 imagery **(C)** and a comparison between pixels and objects for both types of imagery using true mangrove and mangrove associate classes **(D)**.

(A) Quickbird

	AC	MZ	OV	BW	RM	WM	BM
AC		1.892	1.342	1.455	1.837	1.703	1.543
MZ	1.892		1.734	1.690	1.593	1.814	1.355
OV	1.342	1.734		0.994	1.725	1.673	1.233
BW	1.455	1.690	0.994		1.256	1.185	0.702
RM	1.837	1.593	1.725	1.256		0.508	1.129
WM	1.703	1.814	1.673	1.185	0.508		1.258
BM	1.543	1.355	1.233	0.702	1.129	1.258	

(B) Worldview-2

	AC	MZ	OV	BW	RM	WM	BM
AC		**1.963**	1.647	1.698	1.820	1.498	1.785
MZ	**1.963**		1.861	**1.925**	**1.900**	**1.943**	1.647
OV	1.647	1.861		1.532	1.622	1.584	1.381
BW	1.698	**1.925**	1.532		1.617	1.336	1.634
RM	1.820	**1.900**	1.622	1.617		0.866	1.226
WM	1.498	**1.943**	1.584	1.336	0.866		1.540
BM	1.785	1.647	1.381	1.634	1.226	1.540	

(C) Difference

	AC	MZ	OV	BW	RM	WM	BM
AC		0.071	0.304	0.243	−0.017	−0.205	0.242
MZ	0.071		0.127	0.235	0.307	0.129	0.292
OV	0.304	0.127		0.537	−0.103	−0.089	0.148
BW	0.243	0.235	0.537		0.361	0.151	0.932
RM	−0.017	0.307	−0.103	0.361		0.358	0.097
WM	−0.205	0.129	−0.089	0.151	0.358		0.282
BM	0.242	0.292	0.148	0.932	0.097	0.282	

(D) Pixel *vs.* Object for TM and MA

	QB	QB w/BR	WV	WV w/ BR
All Veg Points	0.664	1.141	0.734	1.084
Dense Veg Objects	0.839	1.118	1.321	1.665

QB = Quickbird
WV = Worldview-2
BR = Band Ratios

3.2. Classification

The classification is illustrated in Figure 5. Table 5 shows the proportion of each land cover type. For both study areas, lava and ocean are the dominant cover types and coastal vegetation comprises about 5.5 km^2 or 12% and 8% of Puerto Villamil and Cartago images, respectively. The composition of coastal vegetation differs between the two study areas. The Puerto Villamil study area is mostly sparse vegetation with mangrove associates and true mangroves comprising a minority of coastal vegetation. The Cartago study area is mostly true mangroves with much less sparse vegetation and

almost no mangrove associate species present. However, much of the dense coastal vegetation was obstructed by clouds or cloud shadow in the Worldview-2 image (24.8%).

Figure 5. Land cover classification for Puerto Villamil **(top)** and Cartago **(bottom)**.

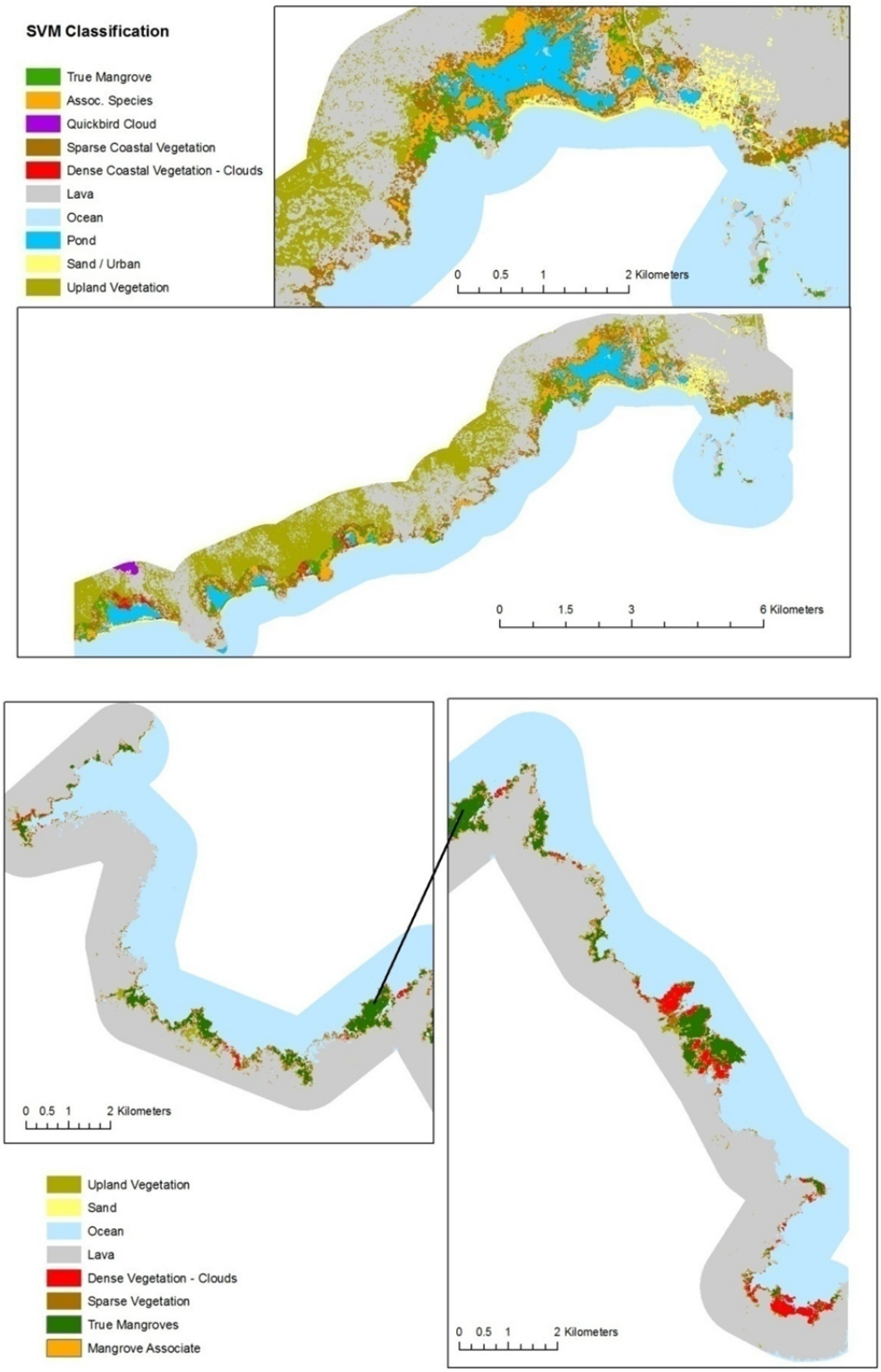

The satellite classification has shown that true mangroves are widespread and the dominant vegetation cover in the Cartago study area, while true mangroves are part of a wider range of

vegetation in the Puerto Villamil study area. In both study areas, mangroves grow along the sheltered coastline and thrive where there is likely subsurface freshwater from the humid highlands emerging along the coast as springs. Several of these springs are found near the town of Puerto Villamil and these reflect the large dense mangrove patches observed.

Table 5. Land Cover Classification for all classes **(A)** and coastal vegetation **(B)**.

(A)

	Puerto Villamil		Cartago	
Cover	**Area**	**Percent**	**Area**	**Percent**
OC	17.9304	38.1463	29.2249	43.4184
PD	1.5400	3.2763	*	
LV	14.1150	30.0291	32.4511	48.2114
SD	0.8032	1.7087	0.0397	0.0589
UV	6.8491	14.5712	0.2722	0.4043
QBC	0.0985	0.2096	0.0000	0.0000
SCV	2.8796	6.1262	1.2552	1.8648
DCVC	0.1785	0.3798	1.0119	1.5033
MA	1.5091	3.2106	0.0006	0.0009
TM	1.1010	2.3423	3.0544	4.5379
Total	47.004	12.0588	67.310	7.9069

(B) Coastal vegetation classes and total.

	Puerto Villamil		Cartago	
Cover	**Area**	**Pct CV**	**Area**	**Pct CV**
SCV	2.8796	0.5080	1.2552	0.2358
DCVC	0.1785	0.0315	1.0119	0.1901
MA	1.5091	0.2662	0.0006	0.0001
TM	1.1010	0.1942	3.0544	0.5739
Total	5.668		5.322	

OC = Ocean
PD = Pond
LV = Lava
SD = Sand
TM = True Mangrove
UV = Upland Vegetation
QBC = Quickbird Clouds
SCV = Sparse Coastal Veg
DCVC = Dense Coast Vegetation w/Clouds
MA = Mangrove Associates

The differences in land cover reflect the differences in the climatic and geomorphic environment. The Puerto Villamil study area is along the southern edge of the Sierra Negra volcano and has considerably more cloud cover during the year than the Cartago study area (unpublished MODIS data). Furthermore, elevation increases rapidly from the coast to the area west of Puerto Villamil, where mists and fog increase with elevation providing moisture to plants. In the Cartago study area, the elevation remains near sea-level with little available moisture, as observed from the barren lava beds, except along the coast where there are likely isolated fresh water springs fed by rain in the humid highlands on Sierra Negra.

Another major difference between the two study areas is the presence of ponds and lagoons. The Puerto Villamil study area contains the largest lagoon system in the Galapagos Islands. The hydrologic connectivity of these lagoons is complex as some lagoons are hyper-saline and others are nearly fresh water [41]. The ranges of hydrologic conditions near Puerto Villamil are likely the cause of the range of vegetation types (*i.e.*, true mangroves *vs.* mangrove associates) and vegetation conditions (*i.e.*, LAI and canopy height) observed. As Song *et al.* [42] observed in this study area, salinity can have an observable impact on remote sensing-derived photosynthetic productivity.

The lagoon complex is the result of volcanic topographic features seemingly unique to that area. In contrast, the structure of the Cartago coastline reflects a more fluvial pattern of inter-tidal channels. The relatively simple topography and hydrology and more arid environment near Cartago has led to isolated but large, dense mangrove patches around protected coves and likely fresh water springs. Future research is needed to investigate the link between hydrologic conditions including subsurface flow and coastal vegetation.

3.3. Accuracy Assessment

The accuracy assessment was considered at two levels: (1) validation objects for a typical assessment of just the SVM classification, and (2) validation field points to understand the accuracy from the decision tree classification and the sub-object level.

3.3.1. SVM

The overall accuracy of the SVM classification between true mangroves and mangrove associates was 94.4% with a kappa statistic of 0.863. The greatest source of error was the misclassification of mangrove associates as true mangroves (Table 6). The producer's and user's error were consistent for each class and greater than 90% in all cases. The AUC-ROC was 0.991 for true mangroves and 0.987 for mangrove associates. The overall accuracy of the classification was very good and better than most previous mangrove studies [4] and thus demonstrates the ability of this approach to accurately distinguish between true and associate mangroves in fringe and basin environments.

Table 6. Classification confusion matrix **(A)** and classification accuracy **(B)** of SVM classification.

(A)	TM (Pix)	TM (%)	MA (Pix)	MA (%)	Total
Unclassified	0	0	0	0	0
TM	3,152	96.04	128	9.69	3,280
MA	130	3.96	1,193	90.31	1,323
Total	3,282	100	1,321	100	4,603

(B)	Prod. (Pix)	Prod.(%)	User (Pix)	User (%)
TM	3,152/3,282	96.04	3,152/3,280	96.1
MA	1,193/1,321	90.31	1,193/1,323	90.17

3.3.2. Total Classification *vs.* Field Points

Table 7 shows the distribution of validation vegetation field data points (*i.e.*, points that did not fall within objects used for the SVM classification). The majority of field points were classified either as sparse coastal vegetation or lava. This is indicative of the arid environment of the study area, particularly in an OBIA classification framework where the spectral signature of the object and not individual pixels are used for classification. Furthermore, given the sparse nature of the vegetation, the spectral signal strength of these vegetation points was relatively weak, preventing further classification with detailed spectral unmixing, requiring hypersepctral data. Of the true mangrove species, about 50% of red and black mangroves points were classified as sparse vegetation, while nearly all of the white mangrove points were classified as sparse. It should be noted that since the field sampling scheme was opportunistic due to Galapagos National Park regulations about cutting vegetation, sampling was likely biased towards less dense and more accessible vegetation, especially for the field plots.

Table 7. Accuracy Assessment of Decision Tree and SVM Classification from Field Data by number of points **(A)** and percent of points **(B)**.

		Remote Sensing Classes										
	(A)	TM	MA	QBC	SCV	DCVC	LV	OC	PD	SD	UV	Total
	AC	2	0	0	18	0	11	0	0	0	0	31
	MZ	5	27	0	2	0	0	0	0	0	0	34
Field	OV	4	9	0	14	0	10	0	0	0	0	37
Data	BW	18	6	0	52	0	12	0	4	0	0	92
Classes	RM	84	8	0	71	0	23	1	18	0	0	205
	WM	43	1	0	159	0	120	7	7	0	0	337
	BM	9	22	0	16	0	6	0	0	0	0	53
	Total	165	73	0	332	0	182	8	29	0	0	789

		Remote Sensing Classes										
	(B)	TM	MA	QBC	SCV	DCVC	LV	OC	PD	SD	UV	Total
	AC	6.45	0.00	0.00	58.06	0.00	35.48	0.00	0.00	0.00	0.00	100
	MZ	14.71	79.41	0.00	5.88	0.00	0.00	0.00	0.00	0.00	0.00	100
Field	OV	10.81	24.32	0.00	37.84	0.00	27.03	0.00	0.00	0.00	0.00	100
Data	BW	19.57	6.52	0.00	56.52	0.00	13.04	0.00	4.35	0.00	0.00	100
Classes	RM	40.98	3.90	0.00	34.63	0.00	11.22	0.49	8.78	0.00	0.00	100
	WM	12.76	0.30	0.00	47.18	0.00	35.61	2.08	2.08	0.00	0.00	100
	BM	16.98	41.51	0.00	30.19	0.00	11.32	0.00	0.00	0.00	0.00	100
	Total	0.209	0.093	0	0.421	0	0.231	0.010	0.037	0	0	1

Figure 6 shows the fuzzy SVM true mangrove classification distribution for each vegetation type. Manzanillo, other vegetation, red mangrove, and white mangrove had appropriate membership to true mangroves. However, black mangrove and buttonwood had low and high membership, respectively, indicating misclassification of these vegetation types.

There are many aspects to this error. First, there is a spatial scale mismatch between the field points and the objects in that many points may occur in a single object. For example, field plots dominated by black mangroves (~11 of 29 dense black mangrove points) were misclassified as mangrove associates due to the misclassification of a single object. Moreover, single points may not be representative of a whole object, not to mention the inherent geometric error in both the field data and remote sensing imagery that may results in a data classification mismatch. Second, fuzzy classification or mixed classes were not explicitly considered. Only pure objects were used for calibrating the classification as the exact composition of mixed objects was unknown due to the lack of a tree census. While mangroves often have detectable patterns of zonation, this is not always observed [43]. This was certainly the case in some parts of the study area where edaphic and topographic conditions changed rapidly over small distance such that for a given field plot, multiple species were present.

Figure 6. Boxplot of true mangrove (TM) fuzzy membership for validation field points.

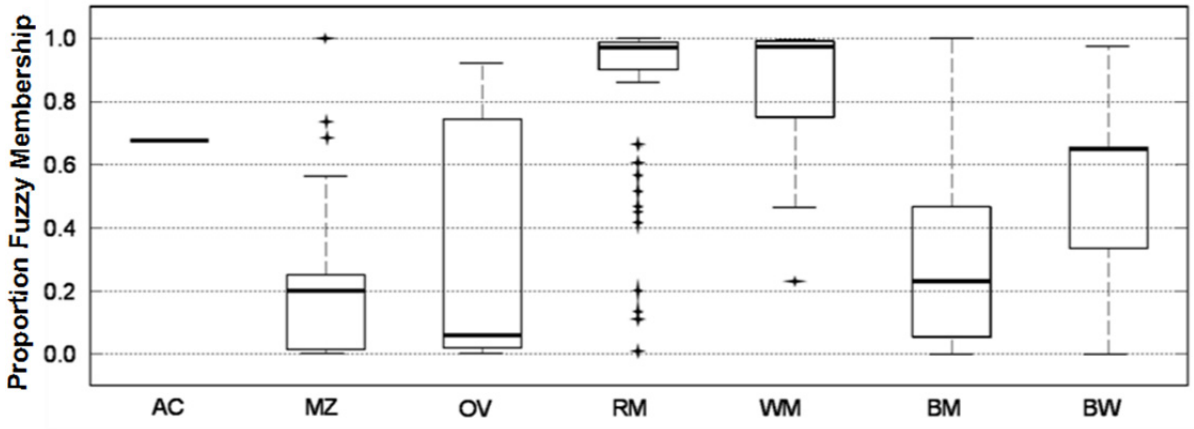

This second point demonstrates a gap in the current knowledge of methods in remote sensing. While there are several papers that assess methods of image segmentation and object classification [44], there is not a good assessment of linking field sampling schemes with OBIA of natural landscapes where visual interpretation is not as straight forward as human landscapes (e.g., buildings, roads, impervious surfaces). Field sampling protocols for remote sensing have been largely designed for pixel-based analysis from a legacy of 25-m pixels from Landsat and SPOT. The type of sampling for pixel based analysis does not lend itself to assessing whole objects created after field data collection, especially fuzzy membership of heterogeneous objects. Two alternative sampling schemes such as large-scale quadrat sampling or mapping boundaries of homogeneous patches may be more appropriate of OBIA, but this type of field data collection is difficult and time-consuming in the best of conditions, let alone in dense mangrove swamps. Another alternative is the visual interpretation of ultra-high resolution (*i.e.*, pixel size less than 5 cm) airborne imagery for a small subset of the study area to generate calibration/validation data. Recent advancements in radio-controlled helicopter platforms are particularly promising for this application. Furthermore, this type of sampling would be prohibitively destructive in the Galapagos National Park. Future research is needed to assess effective and efficient field sampling schemes for use with OBIA.

4. Conclusions

Effective monitoring and management of mangrove forests requires accurate and repeatable measures of forest extent and species composition. While previous studies have successfully mapped mangrove extent and species, these studies have largely ignored fringe mangroves. This study has addressed this issue. Spectral separability analysis revealed that the spectral signatures between mangrove species and even associate species were moderately separable using Quickbird or Worldview-2 imagery at both the pixel and object level. The best separability was found using dense vegetation objects, indicating that even for very high resolution imagery, the multispectral signature of non-vegetation components for sparse vegetation produce mixed pixel effects that seriously limit multispectral analysis. Using a hybrid decision-tree and SVM approach, true mangrove species and associate mangrove species were classified with an accuracy of 94% at the object level. However, when the classification was assessed at the species level, the accuracy was poor for some species such as black and buttonwood mangrove, which had accuracies of 29% and 25%, respectively. This research demonstrates that while non-linear machine-learning classification techniques such as support vector machine, in combination with OBIA of very-high spatial resolution data, can provide marked improvement in the classification of vegetation types, there is a necessity for greater spectral resolution to distinguish between the subtle differences between individual species. Given these findings, future research should focus on hyperspectral image analysis to improve spectral separability between species and LiDAR to enhance image segmentation based on canopy structure as well as spectral properties.

Acknowledgements

This research was supported by a Doctoral Dissertation Research Improvement Grant from the National Science Foundation (Award 0927164), the Center for Galapagos Studies and the Department of Geography at the University of North Carolina at Chapel Hill. The Galapagos National Park and Charles Darwin Research Station provided support in the field. Special thanks to Stephen J. Walsh, Conghe Song, Aaron Moody, Dean Urban, George P. Malanson, and the anonymous reviewers for comments on the manuscript.

References

1. Hogarth, P. *The Biology of Mangroves and Seagrasses*; Oxford University Press: Oxford, UK; New York, NY, USA, 2007.
2. Alongi, D.M. Present state and future of the world's mangrove forests. *Environ. Conserv.* **2002**, *29*, 331.
3. Giri, C.; Ochieng, E.; Tieszen, L.L.; Zhu, Z.; Singh, A.; Loveland, T.; Masek, J.; Duke, N. Status and distribution of mangrove forests of the world using earth observation satellite data. *Global Ecol. Biogeogr.* **2011**, *20*, 154-159.
4. Heumann, B. Satellite remote sensing of mangrove forests: Recent advances and future opportunities. *Progr. Phys. Geogr.* **2011**, *35*, 87-108.
5. Kuenzer, C.; Bluemel, A.; Gebhardt, S.; Quoc, T.V.; Dech, S. Remote sensing of mangrove ecosystems: A review. *Remote Sens.* **2011**, *3*, 878-928.

6. Al Habshi, A.; Youssef, T.; Aizpuru, M.; Blasco, F. New mangrove ecosystem data along the UAE coast using remote sensing. *Aquat. Ecosyst. Health Manage.* **2007**, *10*, 309-319.
7. Benfield, S.L.; Guzman, H.M.; Mair, J.M. Temporal mangrove dynamics in relation to coastal development in Pacific Panama. *J. Environ. Manage.* **2005**, *76*, 263.
8. Gao, J. A hybrid method toward accurate mapping of mangroves in a marginal habitat from SPOT multispectral data. *Int. J. Remote Sens.* **1998**, *19*, 1887-1899.
9. Simard, M.; De Grandi, G.; Saatchi, S.; Mayaux, P. Mapping tropical coastal vegetation using JERS-1 and ERS-1 radar data with a decision tree classifier. *Int. J. Remote Sens.* **2002**, *23*, 1461-1474.
10. Manson, F.J.; Loneragan, N.R.; McLeod, I.M.; Kenyon, R.A. Assessing techniques for estimating the extent of mangroves: Topographic maps, aerial photographs and Landsat TM images. *Mar. Freshwater Res.* **2001**, *52*, 787-792.
11. Ramsey, E.W.; Jensen, J.R. Remote sensing of mangrove wetlands: Relating canopy spectra to site-specific data. *Photogramm. Eng. Remote Sensing* **1996**, *62*, 939.
12. Vaiphasa, C.; Ongsomwang, S.; Vaiphasa, T.; Skidmore, A.K. Tropical mangrove species discrimination using hyperspectral data: A laboratory study. *Estuar. Coast. Shelf Sci.* **2005**, *65*, 371-379.
13. Wang, L.; Sousa, W.P. Distinguishing mangrove species with laboratory measurements of hyperspectral leaf reflectance. *Int. J. Remote Sens.* **2009**, *30*, 1267-1281.
14. Neukermans, G.; Dahdouh-Guebas, F.; Kairo, J.G.; Koedam, N. Mangrove species and stand mapping in GAzi bay (Kenya) using Quickbird satellite imagery. *J. Spat. Sci.* **2008**, *53*, 75-86.
15. Wang, L.; Sousa, W.P.; Gong, P. Integration of object-based and pixel-based classification for mapping mangroves with IKONOS imagery. *Int. J. Remote Sens.* **2004**, *25*, 5655-5668.
16. Wang, L.; Silvan-Cardenas, J.L.; Sousa, W.P. Neural network classification of mangrove species from multi-seasonal ikonos imagery. *Photogramm. Eng. Remote Sensing* **2008**, *74*, 921-927.
17. Huang, X.; Zhang, L.P.; Wang, L. Evaluation of morphological texture features for mangrove forest mapping and species discrimination using multispectral IKONOS imagery. *IEEE Geosci. Remote Sens. Lett.* **2009**, *6*, 393-397.
18. Vaiphasa, C.; Skidmore, A.K.; de Boer, W.F. A post-classifier for mangrove mapping using ecological data. *ISPRS J. Photogramm.* **2006**, *61*, 1-10.
19. Wang, L.; Sousa, W.P.; Gong, P.; Biging, G.S. Comparison of IKONOS and QuickBird images for mapping mangrove species on the Caribbean coast of Panama. *Remote Sens. Environ.* **2004**, *91*, 432-440.
20. Myint, S.W.; Giri, C.P.; Le, W.; Zhu, Z.L.; Gillette, S.C. Identifying mangrove species and their surrounding land use and land cover classes using an object-oriented approach with a lacunarity spatial measure. *GISci. Remote Sens.* **2008**, *45*, 188-208.
21. Krause, G.; Bock, M.; Weiers, S.; Braun, G. Mapping land-cover and mangrove structures with remote sensing techniques: A contribution to a synoptic GIS in support of coastal management in North Brazil. *Environ. Manage.* **2004**, *34*, 429-440.
22. Tomlinson, P.B. *The Botany of Mangroves*; Cambridge University Press: Cambridge, UK; New York, NY, USA, 1986; p. 413.

23. Woodcock, C.E.; Strahler, A.H. The factor of scale in remote sensing. *Remote Sens. Environ.* **1987**, *21*, 311-332.
24. Benz, U.C.; Hofmann, P.; Willhauck, G.; Lingenfelder, I.; Heynen, M. Multi-resolution, object-oriented fuzzy analysis of remote sensing data for GIS-ready information. *ISPRS J. Photogramm.* **2004**, *58*, 239-258.
25. Chubey, M.S.; Franklin, S.E.; Wulder, M.A. Object-based analysis of IKONOS-2 imagery for extraction of forest inventory parameters. *Photogramm. Eng. Remote Sensing* **2006**, *72*, 383-394.
26. Desclee, B.; Bogaert, P.; Defourny, P. Forest change detection by statistical object-based method. *Remote Sens. Environ.* **2006**, *102*, 1-11.
27. Hay, G.J.; Castilla, G.; Wulder, M.A.; Ruiz, J.R. An automated object-based approach for the multiscale image segmentation of forest scenes. *Int. J. Appl. Earth Obs. Geoinf.* **2005**, *7*, 339-359.
28. Wulder, M.A.; White, J.C.; Hay, G.J.; Castilla, G. Towards automated segmentation of forest inventory polygons on high spatial resolution satellite imagery. *Forest. Chron.* **2008**, *84*, 221-230.
29. Conchedda, G.; Durieux, L.; Mayaux, P. Object-Based Monitoring of Land Cover Changes in Mangrove Ecosystems of Senegal. In *Proceedings of 4th International Workshop on the Analysis of Multi-Temporal Remote Sensing Images*, Louvain, Belgium, 18–20 July 2007; pp. 44-49.
30. Pal, M.; Mather, P.M. Support vector machines for classification in remote sensing. *Int. J. Remote Sens.* **2005**, *26*, 1007-1011.
31. Vapnik, V. *The Nature of Statistical Learning Theory*; Springer: New York, NY, USA, 1995.
32. Huang, C.; Davis, L.S.; Townshend, J.R.G. An assessment of support vector machines for land cover classification. *Int. J. Remote Sens.* **2002**, *23*, 725-749.
33. Hsu, C.; Cahng, C.; Lin, C. *A Practical Guide to Support Vector Classification*; Department of Computer Science, National Taiwan University: Taipei, Taiwan, 2010.
34. Yang, X. Parameterizing Support Vector Machines for Land Cover classification. *Photogramm. Eng. Remote Sensing* **2011**, *77*, 27-38.
35. Foody, G.M.; Mathur, A. The use of small training sets containing mixed pixels for accurate hard image classification: Training on mixed spectral responses for classification by a SVM. *Remote Sens. Environ.* **2006**, *103*, 179-189.
36. Li, H.T.; Gu, H.Y.; Han, Y.S.; Yang, J.H. Object-oriented classification of high-resolution remote sensing imagery based on an improved colour structure code and a support vector machine. *Int. J. Remote Sens.* **2010**, *31*, 1453-1470.
37. Van Der Werff, H.H.; Adsersen, H. Dry coastal ecosystems of the Galapagos Islands. In *Dry Coastal Ecosystems: Africa, America, Asia and Oceania*; van der Maarel, E., Ed.; Ecosystems of the World 2B; Elsevier Science Ltd.: Amsterdam, The Netherlands, 1993; pp. 459-475.
38. Schmidt, K.S.; Skidmore, A.K. Spectral discrimination of vegetation types in a coastal wetland. *Remote Sens. Environ.* **2003**, *85*, 92-108.
39. Swain, P. Remote sensing. In *The Handbook of Pattern Recognition and Processing*; Young, T., Fu, K., Eds.; Academic Press: Orlando, FL, USA, 1986; pp. 613-627.
40. Metz, C.E. Basic principles of ROC analysis. *Semin. Nucl. Med.* **1978**, *8*, 283-298.
41. Song, C.; White, B.; Heumann, B.W. Hyperspectral remote sensing of salinity stress on red (*Rhizophora mangle*) and white (*Laguncularia racemosa*) mangroves on Galapagos Islands. Unpublished data.

42. Song, C.; White, B.; Heumann, B. Hyperspectral remote sensing of salinity stress on red (*Rhizophora mangle*) and white (*Laguncularia racemosa*) mangroves on Galapagos Islands. *Remote Sens. Lett.* **2011**, *2*, 221-230.
43. Ward, G.A.; Smith, T.J.; Whelan, K.R.T.; Doyle, T.W. Regional processes in mangrove ecosystems: Spatial scaling relationships, biomass, and turnover rates following catastrophic disturbance. *Hydrobiologia* **2006**, *569*, 517.
44. Blaschke, T.; Lang, S.; Hay, G. *Object-Based Image Analysis: Spatial Concepts for Knowledge-Driven Remote Sensing Applications*; Springer: Berlin/Heidelberg, Germany, 2008.